Increasing Mo^{5+} in M-doped La$_2$(MoO$_4$)$_3$ (M=Fe, Co, Ni, Cu, and Zn) toward efficient electrocatalytic nitrogen fixation

Liangqing Hu [a], Yanming Guo [a], Jin Chang [b] *, Yinpeng Lu [a], Xiaojiang Su [a], Xinyi Zhang [a], Di Geng [a], Yueming Ren [a], Tong Wei [a], Hexin Zhang [a] *, Jing Feng [a] *

[a] *Key Laboratory of Superlight Materials & Surface Technology of Ministry of Education, Harbin Engineering University, Harbin 150001, PR China*

[b] *Taiyuan University of Science and Technology, College of Energy and Materials Engineering, 300024*

* Corresponding author. Tel: +86-451- 82569890, Fax: +86-451-82533026.

E-mail address: fengjing@hrbeu.edu.cn (J Feng), zhanghx@hrbeu.edu.cn (HX Zhang), changjin621@163.com (J Chang)

1. Characterization

The structure was investigated by X-ray diffraction (XRD, Rigaku/TTR- III with Cu-Kα radiation, λ =1.66 nm) with a tube voltage of 30 KV. The Brunauer-Emmett-Teller (BET, Tristar II 3020) surface areas of the samples were measured at 77 K using Autosorb-iQ. The functional groups were characterized by Fourier-transform infrared spectra (FT-IR, Perkin-Elmer 580B). The microstructure and crystal structure of the samples were characterized by scanning electron microscopy (SEM, SU70-HSD,20 kV) and transmission electron microscopy (TEM, FEI Tecnai TF20, 120 kV). The chemical composition was analyzed using X-ray photoelectron spectroscopy (XPS, PHI 5700) with monochromatic Al Kα irradiation. The absorbance data were measured with UV–vis absorption spectroscopy (UV-752G). All electrochemical measurements were carried out three times on a CHI660D workstation (Shanghai Chenhua Instrument Co. Ltd, China) at room temperature in a three-electrode system, with an Ag/AgCl electrode in 0.1 mol L^{-1} Na_2SO_4 electrolyte as the reference, a carbon rod as the counter electrode, and a platinum foil $(1 \times 1 \text{ cm}^2)$ as the working electrode. Each electrochemical experiment was repeated three times.

2. Preparation of working electrode

Catalyst (9.5 mg) and carbon nanotubes (0.5 mg) were distributed in 485 μL deionized water, 485 μL alcohol, and 30 μL 5 wt.% Nafion solution. After sonication for 30 min, the homogeneous liquid was formed. Finally, the liquid (45 μL) was accurately measured and evenly painted on the carbon paper that had been pre-treated.

(Containing 0.4275 mg catalyst and 0.0225 mg carbon nanotubes). The painted carbon paper was left to dry and used for subsequent electrochemical tests.

3. Electrochemical testing

In this paper, the electrocatalytic nitrogen reduction performance measurements were tested on a CHI660D workstation (Shanghai Chenhua Instrument Co. Ltd., China) at room temperature. In a three-electrode system, a carbon paper painted with catalyst, an Ag/AgCl electrode, and a carbon rod were used as the working electrode (1×1 cm^2), the reference, and the counter electrode, respectively in 0.1 mol L^{-1} Na$_2$SO$_4$ solution [S1]. Noteworthy, the Ag/AgCl reference electrode was converted to the RHE reference scale by

$$E \text{ (vs. RHE)} = E_0 \text{(Ag/AgCl)} + E \text{ (Ag/AgCl)} + 0.0591 \times pH \qquad (1)$$

(E_0 (Ag/AgCl) $=0.1976$ V).

4. Ammonia quantification

NH$_4$Cl (3.8214 g) was accurately weighed and completely dissolved in 1000 mL of 0.1 mol L^{-1} Na$_2$SO$_4$ solution ($\rho_N = 1000$ μg mL^{-1}). Then, 1 mL of the above solution was placed in 100 mL of 0.1 mol L^{-1} Na$_2$SO$_4$ solution ($\rho_N = 10$ μg mL^{-1}). Subsequently, 0, 0.2, 0.4, 0.6, 0.8, and 1.0 mL of the above solutions were added to 10 mL colorimetric tubes, respectively. After that, 0.1 mol L^{-1} Na$_2$SO$_4$ solution was dropped into the scale. Afterward, 200 μL of potassium sodium tartrate solution and 300 μL of Nessler were added sequentially. After shaking well and standing for 10 min, the absorbance was measured at 420 nm [S2]. The fitted equation of the standard curve was obtained as $A=$

0.167 C + 0.0256 (R^2 = 0.999). Where A is the absorbance of ammonia, C (µg mL^{-1}) is the ammonia concentration of the solution after 2 h of the NRR, and R^2 is the correlation coefficient. The standard curve for different concentrations of NH$_4^+$ solution was displayed in Fig. S1(a).

10 mL electrolyte which had conducted NRR for 2 h, 200 µL potassium sodium tartrate solution, and 300 µL Nessler solution were added to the colorimetric tube in turn. Thereafter, the solution was evenly shaken and allowed to stand for 10 min before measuring the absorbance at 420 nm. The rate of ammonia production was calculated and its formula was

$$NH_{3\ yield\ rate} = (C \times V)/(t \times m) \qquad (2)$$

Where C (µg m L^{-1}) is the ammonia concentration of the solution after 2 h of the NRR, V (mL) is the volume of electrolyte in the cathode chamber (V = 75 mL), t (h) is electrocatalytic NRR for 2 h, an m (mg) is a loading of catalyst at the working electrode [S3].

5. Faradaic efficiency

Faradic efficiency (FE) measures the ratio of the charge required to synthesize NH$_3$ to the charge passing through the electrodes during electrolysis. The FE was calculated as

$$FE = (n \times F \times C \times V)/(17 \times Q) \qquad (3)$$

Where n is the number of electrons needed to synthesize NH$_3$ (taken as 3), F (C mol^{-1}) is Faraday's constant (taken as 96485), C (µg mL^{-1}) is ammonia concentration of the

solution after 2 hours of the NRR, V (mL) is the volume of electrolyte in the cathode chamber (taken as 75 mL), and Q (C) is the amount of charge.

6. Determination of by-products

The by-products generated during the NRR were determined by the Watt-Chrisp method. Initially, 5.99 g ρ-$C_9H_{11}NO$ was dissolved in 30 mL 0.1 mol L^{-1} HCl solution and 300 mL ethanol. The resulting solution was mixed and used as the color developer for N_2H_4. 0.4 mL, 0.6 mL, 0.8 mL, 1.0 mL, and 1.2 mL of the above solutions were added into 10 mL colorimetric tubes, respectively. Then, the solution was titrated with 0.1 mol L^{-1} HCl solution to the scale line. Finally, the absorbance value at 455 nm was measured after shaking well and standing for 15 min. The fitted equation of the standard curve was obtained as

$$A= 0.16775\ C + 0.0063\ (R^2 = 0.999). \tag{4}$$

Where A is the absorbance of ammonia, C (μg mL^{-1}) is the N_2H_4 concentration of the solution after 2 hours of the NRR, and R^2 is the correlation coefficient (Fig.S1 (b)).

After electrocatalytic nitrogen reduction for 2 hours, 5 mL electrolyte, and 5 mL color developer were added sequentially to the colorimetric tube. Subsequently, the above solution was shaken evenly and left for 15 minutes. Finally, the absorbance at 455 nm was measured.

7. Electrochemically active surface area

The electrochemically active surface area (ESCA) was tested by cyclic voltammetry testing and calculated as

$$ECSA = C_{dl}/60.$$
(5)

Where C_{dl} (μF m^{-2}) is bilayer capacitance.

8. Density functional theoretical calculation

All calculations in this work were performed using the Vienna Ab initio Simulation Package (VASP). The ionic cores were represented by projected augmented waves (PAW). The energy was converged to less than 0.01 eV Å^{-1} with a plane wave kinetic energy cutoff of 450 eV. Exchange and correlation effects were incorporated within the generalized gradient approximation (GGA) with Perdew, Burke, and Ernzerhof (PBE) exchange–correlation function. Due to the spurious self-repulsion and the missing derivative discontinuity of transition metal oxides, plain DFT functionals do not accurately describe the electronic structure of these materials. Thus, DFT+U approach of Dudarev with a U-J parameter of 5.5 eV was employed to correct the electronic structure of samples. The calculation used a $3 \times 3 \times 1$ Γ-point-centered Monkhorst-Pack k-point mesh to geometry relaxation, and $30 \times 30 \times 10$ for densities of stages. The lattice parameter of samples is calculated by Materials Studio.
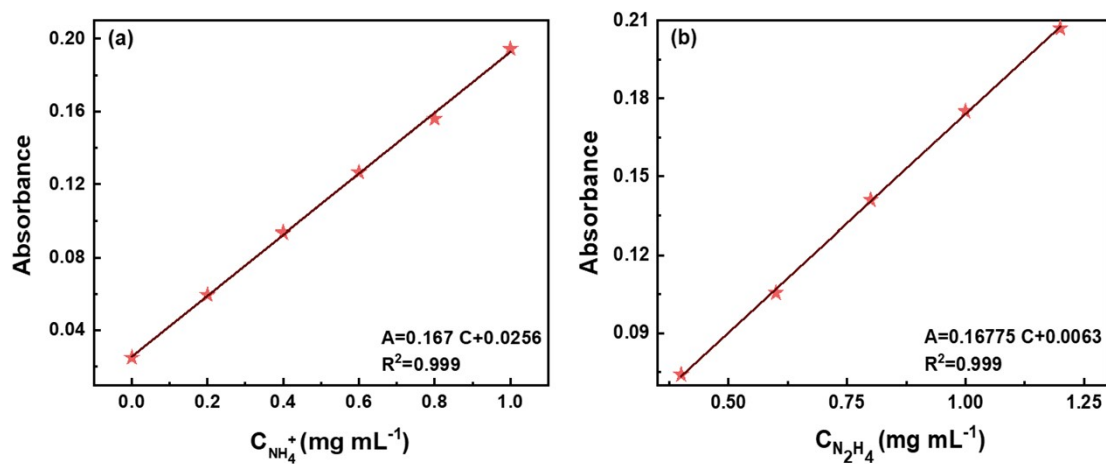
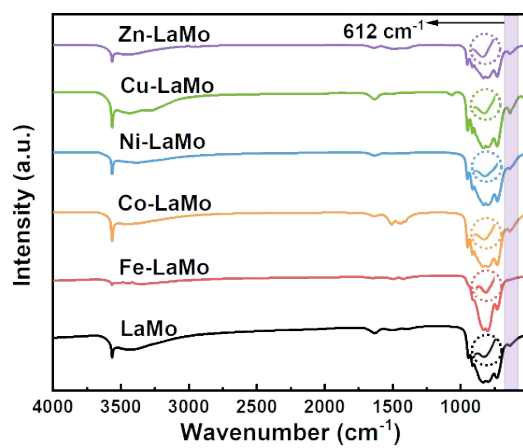Fig. S1 Standard curve of different concentrations of (a) NH_4^+ solution, (b) N_2H_4 solution.

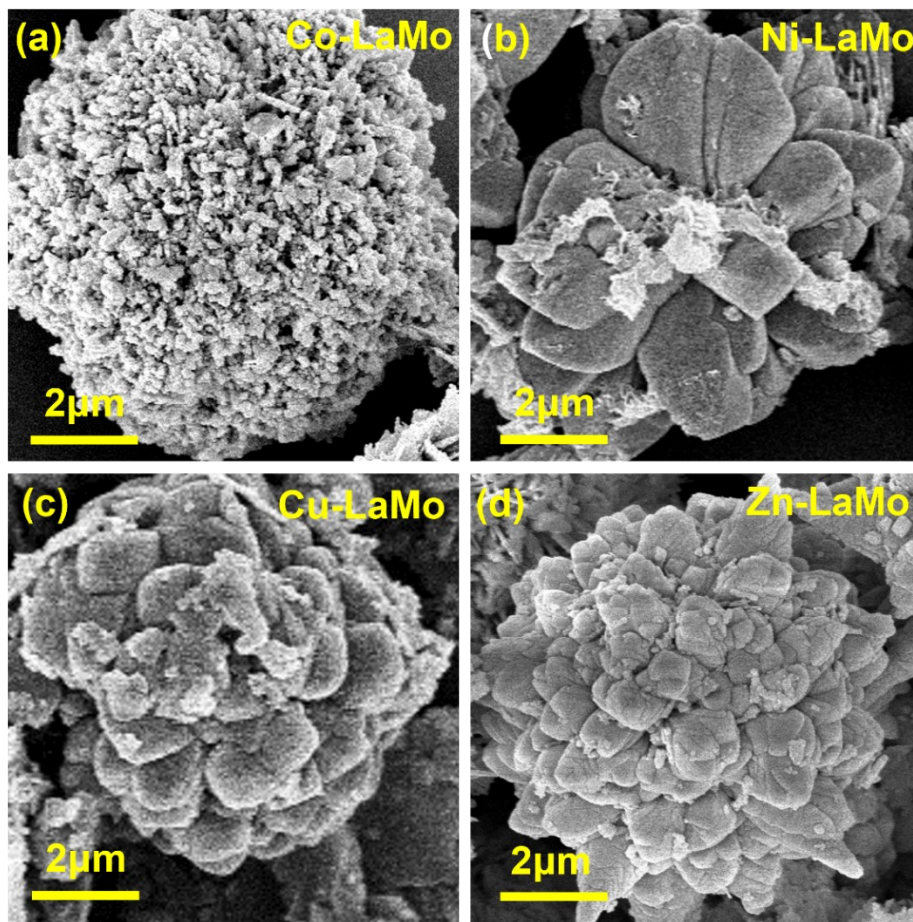Fig. S2 FT-IR of LaMo, and M-LaMo (M= Fe, Co, Ni, Cu, and Zn).

Fig. S3 SEM images of (a) Co-LaMo, (b) Ni-LaMo, (c) Cu-LaMo, (d) Zn-LaMo.

The Fe 2p spectra of Fe-LaMo (Fig.S4 (a)) is assigned to Fe^{3+}(725.6 and 712.3 eV), and Fe^{2+}(723.8 and 710.5 eV) [S4]. Meanwhile, the Co 2p spectra of Co-LaMo (Fig.S4 (b)) is attributed to Co^{3+}(794.7 and 779.5 eV), and Co^{2+} (796.0 and 780.8 eV) [S5]. From the Ni 2p spectra of Ni-LaMo (Fig.S4 (c)), the peaks are attributed to Ni^{2+}(873.0 and 861.9 eV), and satellite peaks (880.1 and 865.9 eV) [S6]. The peaks appearing in the Cu 2p spectra of Cu-LaMo (Fig.S4 (d)) are classified as assigned to Cu^{2+}(955.0 and 935.0 eV) and Cu^{+}(952.2 and 932.2 eV) [S7]. Then, the peaks appearing at 1043.4, and 1023.3 eV are assigned to Zn^{2+} according to the Zn 2p spectra of Zn-LaMo (Fig.S4 (e)) [S8].
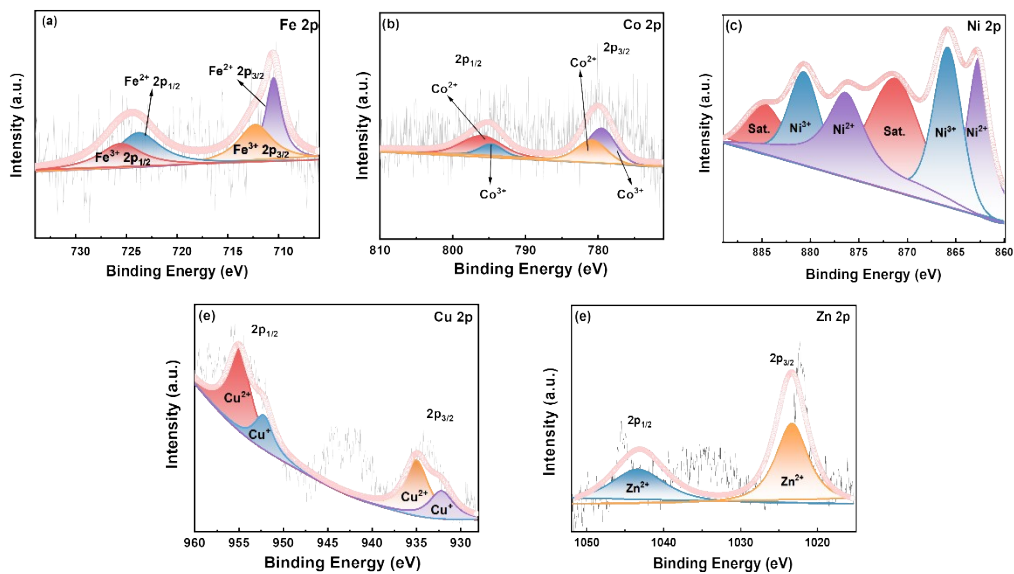
Fig.S4 (a) Fe 2p of Fe-LaMo, (b) Co 2p of Co-LaMo, (c) Ni 2p of Ni-LaMo, (d) Cu 2p of Cu-LaMo, (e) Zn 2p of Zn-LaMo.
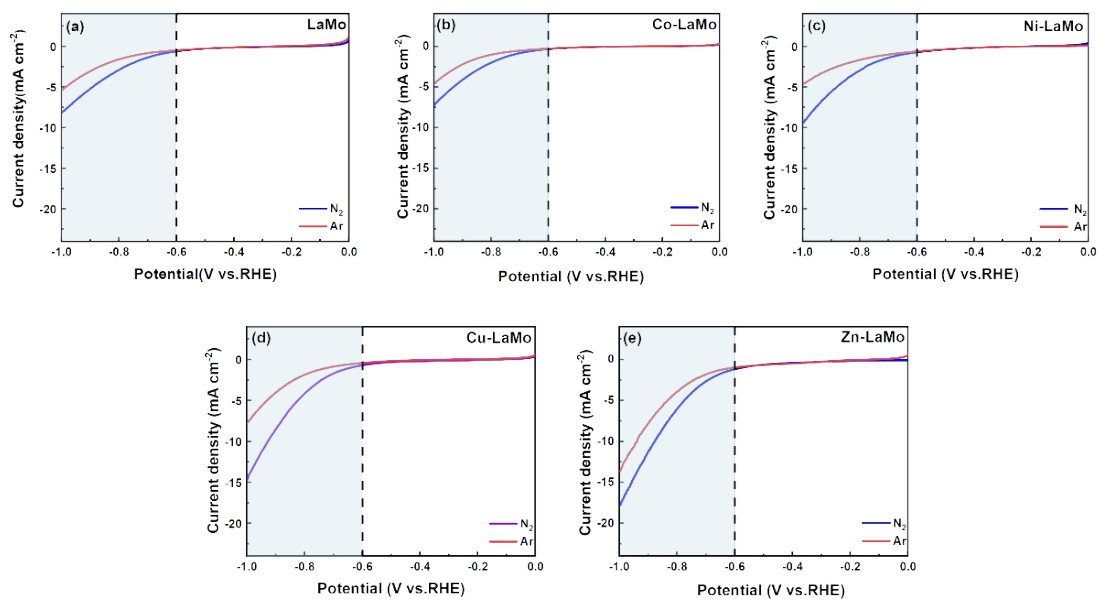

Fig. S5 LSV curves of (a) LaMo, (b) Co- LaMo, (c) Ni- LaMo, (d) Cu-LaMo, and (e) Zn-LaMo.
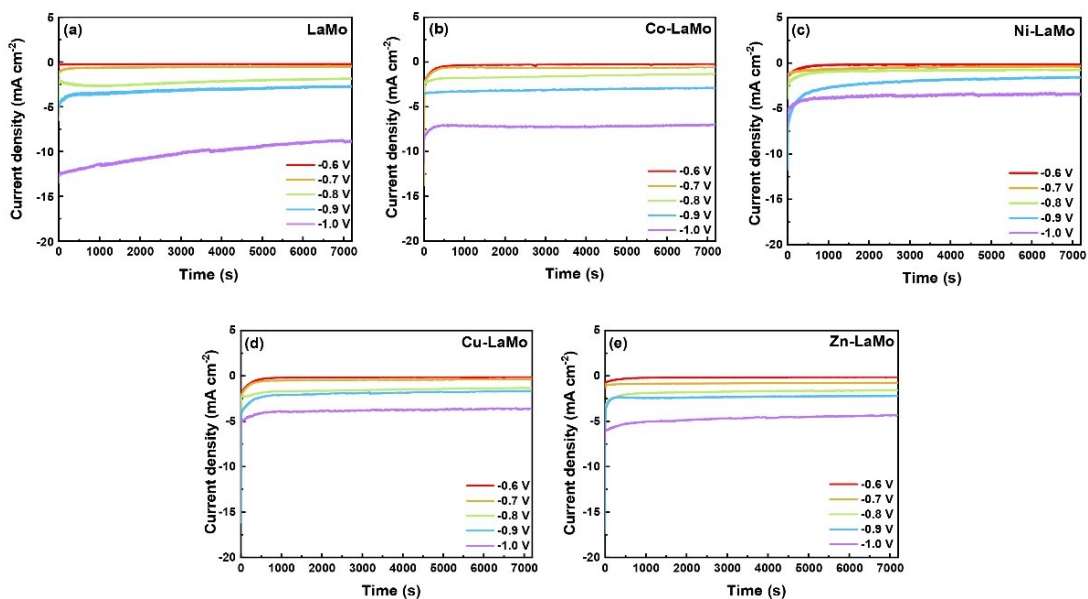
Fig. S6 Chronoamperometric curves at various potentials of (a) LaMo, (b) Co-LaMo, (c) Ni-LaMo,
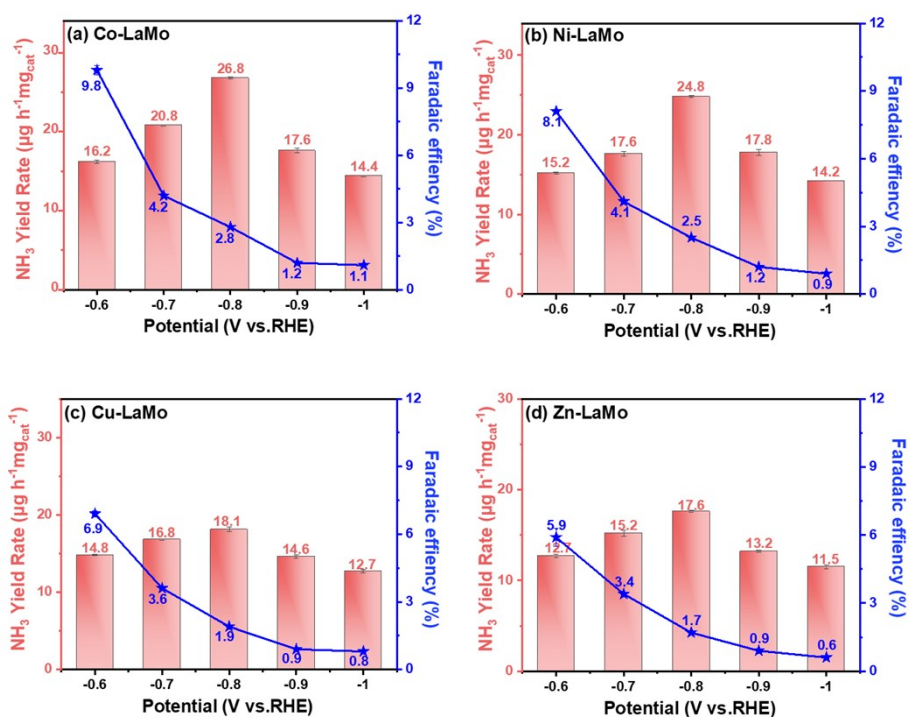
(d) Cu-LaMo, (e) Zn-LaMo.

Fig. S7 The NRR performance of (a) Co-LaMo, (b) Ni-LaMo, (c) Cu-LaMo, (d) Zn-LaMo at
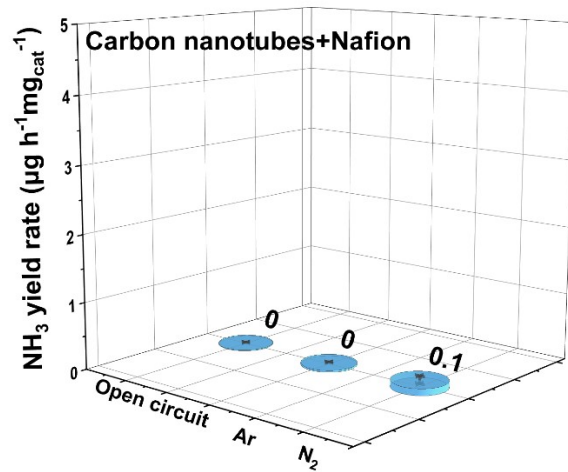
different voltages.

Fig. S8 The NH$_3$ yield rate of Carbon nanotubes and Nafion under different conditions at -0.8 V
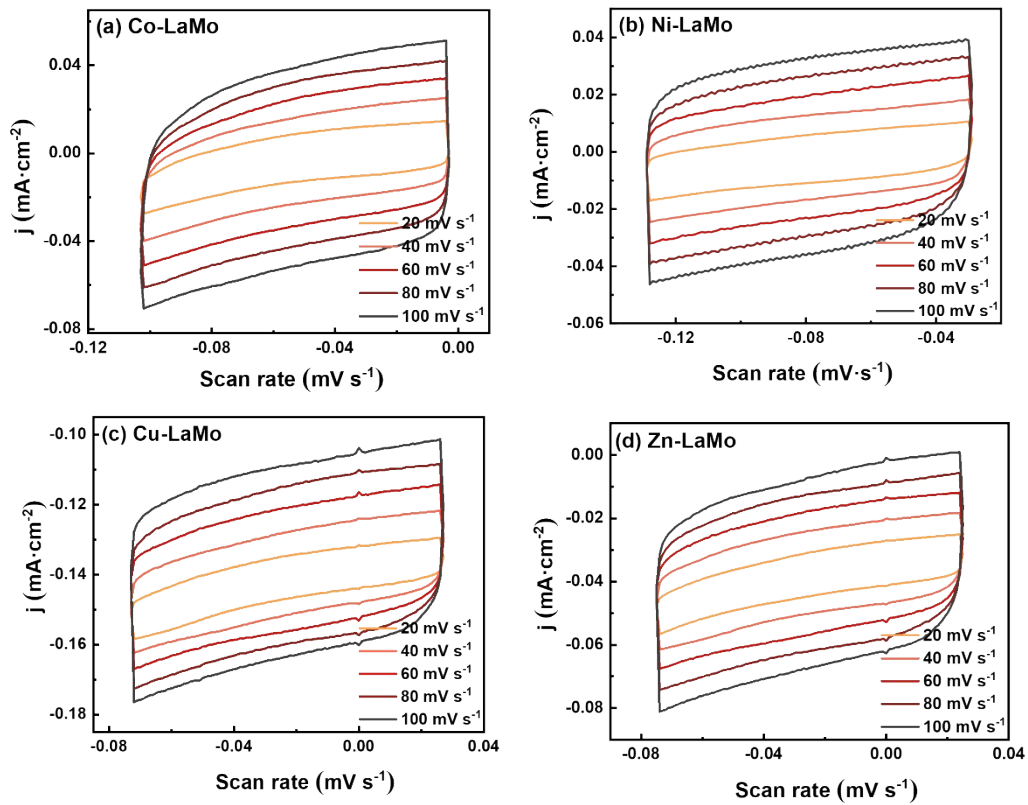
(vs. RHE).

Fig. S9 CV curves of (a) Co-LaMo, (b) Ni-LaMo, (c) Cu-LaMo, (d) Zn-LaMo at different

voltages.

11

Table S1. The ionic radius of elements.

Element	Ionic radius
$r_{Fe^{2+}}$	0.76
$r_{Co^{2+}}$	0.74
$r_{Ni^{2+}}$	0.72
$r_{Cu^{2+}}$	0.72
$r_{Zn^{2+}}$	0.74
$r_{La^{3+}}$	1.06
$r_{Mo^{6+}}$	0.62

Table S2. The lattice parameter of samples.

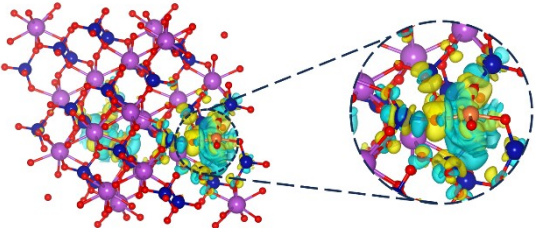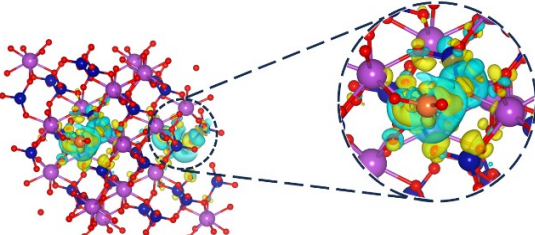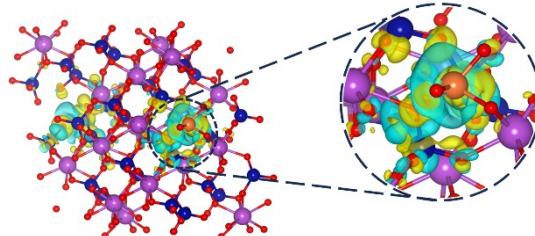| Samples	a (Å)	b (Å)	c (Å)
Fe-LaMo	5.3496	5.3496	11.8059
Co-LaMo	5.3498	5.3498	11.7999
Ni-LaMo	5.3498	5.3498	11.7870
Cu-LaMo	5.3499	5.3499	11.7821
Zn-LaMo	5.3500	5.3500	11.7818
LaMo	5.3506	5.3506	11.7743

Table S3. Comparison of the NRR performances of Fe-LaMo with reported NRR catalysts at ambient conditions.

Catalysts	NH$_3$ yield rate	FE (%)	Ref.
Fe-LaMo	**30.4 µg h^{-1} mg$_{cat}^{-1}$**	**3.6%**	**This work**
Co-LaMo	**26.8 µg h^{-1} mg$_{cat}^{-1}$**	**2.8 %**	**This work**
Ni-LaMo	**24.8 µg h^{-1} mg$_{cat}^{-1}$**	**2.5 %**	**This work**
Cu-LaMo	**18.1 µg h^{-1} mg$_{cat}^{-1}$**	**1.9 %**	**This work**
Zn-LaMo	**17.6 µg h^{-1} mg$_{cat}^{-1}$**	**1.7 %**	**This work**
LaMo	**17.6 µg h^{-1} mg$_{cat}^{-1}$**	**1.5 %**	**This work**
Fe-W$_{18}$O$_{49}$	24.7 µg h^{-1} mg$_{cat}^{-1}$	20.0 %	[S9]
FeMoO$_4$	17.5 µg h^{-1} mg$_{cat}^{-1}$	10.5 %	[S10]
Fe-Doped NiMoO$_4$	15.4 µg h^{-1} mg$_{cat}^{-1}$	26.9 %	[S11]
MoS$_2$ NDs/RGO	16.4 µg h^{-1} mg$_{cat}^{-1}$	27.9%	[S12]
MoO$_3$	29.4 µg h^{-1} mg$_{cat}^{-1}$	1.9 %	[S13]
Mo nanofilm	1.89 µg h^{-1} mg$_{cat}^{-1}$	0.72 %	[S14]

Table S4. Repetitions of electrochemical experiments.

Experiment name	Repeat times
Linear sweep voltammetry (LSV)	3
Chronoamperometric curves	3
NH$_3$ content was determined by Nessler	3
Electrolyzed continuously for 24 h	3
Cycle testing	4
Electrochemical resistance	3
Cyclic voltammetry	3

Table S5. Charge density difference analysis, percentage of Mo^{5+}, absorptive energy and NRR performance of LaMo, and M- LaMo (M= Fe, Co, Ni, Cu, Zn). (Isosurface is set to 0.001 $e/Bohr^3$.)

Catalysts	Charge density difference analysis (The yellow portion and blue portion represent charge accumulation and depletion, respectively.)	The percentage of Mo^{5+} (%)	Absorptive energy (eV)	NH$_3$ yield rate ($\mu g\ h^{-1}\ mg_{cat}^{-1}$)	FE (%)
Fe-LaMo		52	-0.8257	30.4	3.6
Co-LaMo		39	-0.6866	26.8	2.8
Ni-LaMo		32	-0.6639	24.8	2.5

Cu-LaMo

21   -0.6339   18.1   1.9

Zn-LaMo

18   -0.6102   17.6   1.7

LaMo

12   **-0.5984**   **17.6**   **1.5**

La   Mo   O   M (M=Fe , Co , Ni , Cu , Zn)
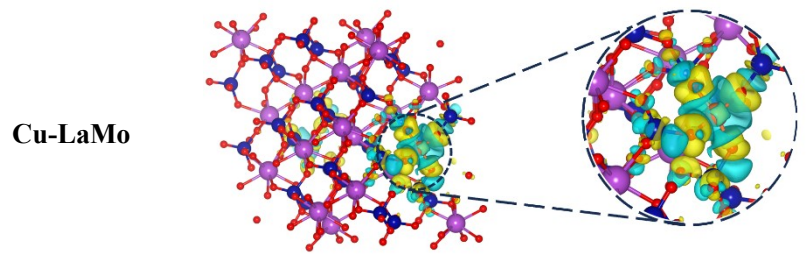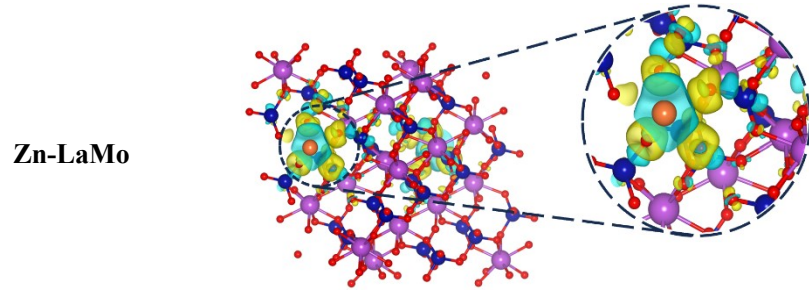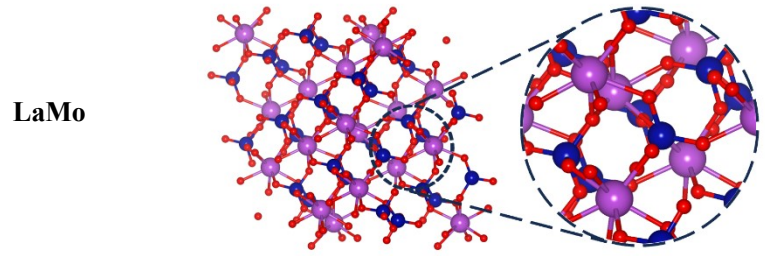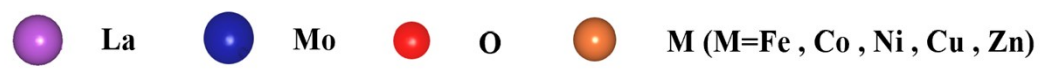
15

REFERENCES

[S1] H Fei, T Guo, Y Xin, et al. Sulfur vacancy engineering of MoS_2 via phosphorus incorporation for improved electrocatalytic N_2 reduction to NH_3 [J]. Applied Catalysis B: Environmental, 2022, 300.

[S2] Kim C, Song J Y, Choi C, et al. Atomic-Scale Homogeneous Ru-Cu Alloy Nanoparticles for Highly Efficient Electrocatalytic Nitrogen Reduction [J]. Advanced Materials, 2022, 34(40).

[S3] R Q Liu, H Fei, J Wang, et al. Insights of active sites separation mechanism for highly efficient electrocatalytic N_2 reduction to ammonia over glucose-induced metallic MoS_2 [J]. Applied Catalysis B: Environmental, 2023, 337.

[S4] G H Liu, L J Niu, Z X Ma, et al. $Fe_2Mo_3O_8$/XC-72 electrocatalyst for enhanced electrocatalytic nitrogen reduction reaction under ambient conditions [J]. Nano Research, 2022, 15(7): 5940-5.

[S5] F Z Sun, C Q Li, B Li, et al. Amorphous MoS_x developed on $Co(OH)_2$ nanosheets generating efficient oxygen evolution catalysts [J]. Journal of Materials Chemistry A, 2017, 5(44): 23103-14.

[S6] D Wu, X B Xie, J J Zhang, et al. Embedding NiS nanoflakes in electrospun carbon fibers containing NiS nanoparticles for hybrid supercapacitors [J]. Chemical Engineering Journal, 2022, 446.

[S7] L Q Hu, K N Liu, Y M Guo, et al. Oxygen vacancies-rich Cu-$W_{18}O_{49}$ nanorods supported on reduced graphene oxide for electrochemical reduction of N_2 to NH_3

[J]. Journal of Colloid and Interface Science, 2023, 644: 285-94.

[S8] Karazmoudeh N J, Soltanieh M, Hasheminiasari M. Structural and photocatalytic properties of undoped and Zn-doped CuO thin films deposited by reactive magnetron sputtering [J]. Journal of Alloys and Compounds, 2023, 947.

[S9] Y Y Tong, H P Guo, D L Liu, et al. Vacancy Engineering of Iron-Doped $W_{18}O_{49}$ Nanoreactors for Low-Barrier Electrochemical Nitrogen Reduction, Angewandte Chemie-International Edition, 2020,59(19) 7356-61.

[S10] J Wu, Z X Wang, S W Li, et al. $FeMoO_4$ nanorods for efficient ambient electrochemical nitrogen reduction [J]. Chemical Communications, 2020, 56(50): 6834-7.

[S11] N Liu, R Wu, Y Liu, et al. Oxygen Vacancy Engineering of Fe-Doped $NiMoO_4$ for Electrocatalytic N_2 Fixation to NH_3 [J]. Inorganic Chemistry, 2023.

[S12] Y Y Liu, W K Wang, S B Zhang, et al. MoS_2 Nanodots Anchored on Reduced Graphene Oxide for Efficient N_2 Fixation to NH_3 [J]. Acs Sustainable Chemistry & Engineering, 2020, 8(5): 2320-6.

[S13] J R Han, X Q Ji, X Ren, et al. MoO_3 nanosheets for efficient electrocatalytic N_2 fixation to NH_3 [J]. Journal of Materials Chemistry A, 2018, 6(27): 12974-7.

[S14] F C Gao, R C Xin, Q W Shun, et al. Ammonia Electrosynthesis with High Selectivity under Ambient Conditions via a Li^+ Incorporation Strategy, Journal of The American Chemical Society. 139(26) (2017) 9771-9774.